PRECIPITATION OF CARBIDES AND SIGMA PHASE IN AISI TYPE 446 STAINLESS STEEL UNDER WORKING CONDITIONS

A.A. Guimarães[1] and P.R.Mei[2]

1. Faculdade de Engenharia Mecânica, Unicamp, Campinas, SP, Brasil; email: adaguima@globo.com
2. Faculdade de Engenharia Mecânica, Unicamp, Campinas, SP, Brasil; email: pmei@fem.unicamp.br

ABSTRACT

The microstructure of tubes of AISI 446 ferritic stainless steels used in a heating furnace of a petrochemical plant was investigated using scanning electron microscopy, energy-dispersive spectrometry, X-ray diffraction, hardness and microhardness measurements. It was found that, under the working conditions the tubes were subjected, precipitation of carbides and sigma phase occurs. Heat treatment does dissolve these precipitates but the tubes cannot be regenerated due to their change in composition, which occurs preferentially at the face of the tubes closest to the flames.

KEYWORDS: Carbides, Sigma Phase, Heat Treatment, Stainless Steel.

1 – INTRODUCTION

Ferritic stainless steels are basically iron-chromium alloys with sufficient chromium and other elements, such as Mo, Si, Al etc., to stabilize the ferrite phase with a body centered cubic (b.c.c.) structure at all temperatures. At room temperature, they consist of chromium-rich alpha (α) solid solution with very little dissolved carbon; the majority of the carbon present in the alloy appears in the form of more or less finely-divided chromium carbides (1). AISI Type 446 steel contains 23 to 27% Cr, the highest Cr content of the commercially available ferritic alloys. Due to its high chromium content, it may exhibit sigma phase after certain heat treatments (2). This alloy has several properties that make it commercially attractive. When annealed, it displays excellent corrosion resistance to a variety of corrosive solutions; it does not undergo stress corrosion cracking in chloride environments; and it has a relatively low cost. However, its corrosion resistance and ductility are severely weakened by high temperature exposures such as welding. Therefore, it has been used as a construction material far less than have the austenitic grades of stainless steel which contain chromium and nickel (1). In situations where the corrosion resistance of austenitic steels is low, the choice of a ferritic steel may be the best alternative. Such is the case for a furnace used to heat process gas in a petrochemical plant in Brazil; such gas has a significant amount of H_2S and several hydrocarbons. Figure 1 shows a schematic of the tube arrangements in the furnace. Further, the entrance temperature of the gas is around 200^{o}C and it must exit the furnace in the range of 530 to 580^{o}C. Thus, the tubes work with temperatures in the range of 200 to 800^{o}C. Despite the fact that the tests in the development stage of the plant showed that the AISI 446 would have an optimal performance, the initial industrial results were poor (3,4). In order to understand what was causing the lower-than-expected results, a series of tests were carried out. In this paper, the microstructures, hardnesses and mechanical properties are reported.

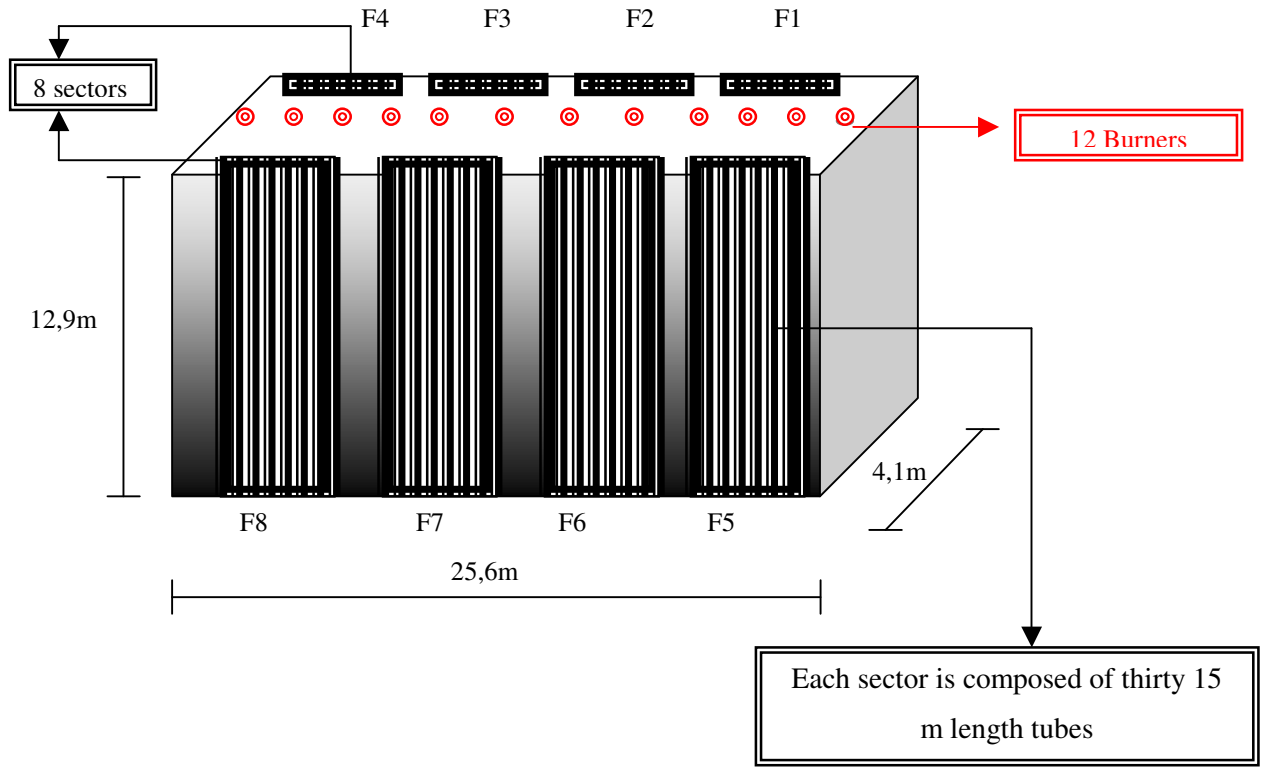

Figure 1 - Schematic of the furnace chamber.

2- EXPERIMENTAL

AISI 446 alloy tubes were manufactured by Sumitomo and supplied to the Brazilian company Petrobrás, to use in the sectors shown in Figure 1. We analyzed new tubes and tubes which were taken from the furnace because they had failed or were about to fail. Table 1 shows the chemical compositions found.

Table1 - Chemical compositions of the AISI 446 tubes.

Sample	Element (wt%)									
	C	Si	Mn	Cr	P	S	N	Ni	Mo	V
New 1	0.088	0.48	0.92	24.13	0.027	0.002	0.24	0.32	<0.05	0.07
New 2	0.089	0.49	0.93	24.30	0.027	0.002	0.24	0.29	<0.05	0.07
Used 1	0.13	0.56	1.01	26.26	0.027	0.006	0.22	0.31	0.09	0.07
Used 2	0.16	0.56	0.67	26.21	0.030	0.012	0.23	0.29	0.10	0.07
Used 3	0.17	0.58	0.69	26.32	0.029	0.009	0.23	0.30	0.10	0.07

Because the process gas travels inside the tubes, a corrosion scale was noticed to form on their internal surfaces. It was decided to verify the chemical composition throughout the tube wall thickness, which was done in two ways: one piece of used tube was cut and flattened to make it possible to analyze the internal surface of the tube gradually while removing material by grinding; another piece of used tube was placed in a lathe and material was removed from the inside and collected for analysis.

Since the scale inside the used tubes was more pronounced on the side facing the furnace interior, another piece of tube was cut into four quarters, flattened and the internal face analyzed in each quarter (see Figure 2). The samples were etched using glyceregia to see the general

microstructure and electrolytic KOH to reveal the presence of any sigma. Micrographs were taken by SEM and the compositions of both the matrix and second phase were determined by EDS. The hardness was measured on the Rockwell B scale with a 100 kgf load and the microhardness of the samples was measured on the HV scale using 20g load.

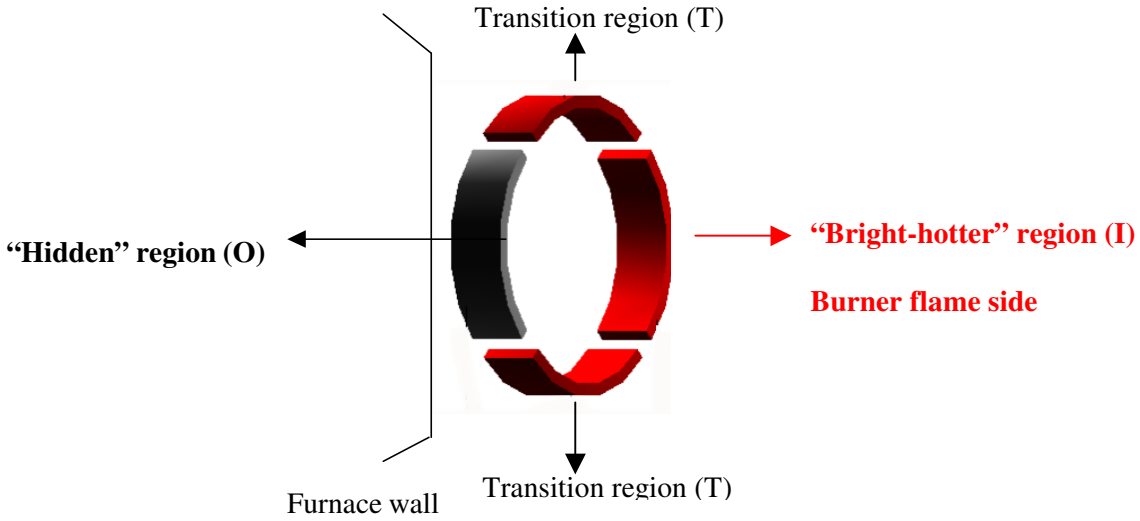

Figure 2 - Schematic of where samples were taken from tube for chemical analysis and metallography.

Heat treatments were carried out to check for microstructural changes of the precipitated particles and to verify if a kind of regeneration is possible in the used tubes. Table 2 shows the treatments performed.

Table 2 – Regeneration heat treatments performed

Sample	Temperature (°C)	Holding time (h)	Cooling
Used 1	850 to 950	1 to 2	Air or water
Used 2	850 to 1100	1 to 108	Air or water
Used 3	900 to 1300	2 to 60	Air

3- RESULTS AND DISCUSSION

3.1- Chemical Analysis

Table 3 shows the results of the analysis carried out in the tube which was flattened to allow analysis by an ARL optical spectrometer and gradually ground to smaller thickness and reanalyzed. The chips removed by machining from the internal part of the tube were also analyzed by direct combustion and the results are also provided in table 3.

The results of the analysis to determine the difference from each quadrant of the tube are given in Table 4. It is of interest that both carburization and sulfidation occur on the internal surface of the tubes; this is explained by the composition of the process gas and the working temperature, which can go as high as 800°C. Since the temperature gradients in the tubes are significant from furnace top and bottom as well as from tube facing furnace interior to furnace wall (a gradient of 120°C was measured using thermometry techniques by Petrobrás (5)), the levels of carbon and sulfur absorption also vary accordingly, as can be noted (Tables 3 to 4). As can be seen, the levels of carbon and sulfur are much higher in the surface layer than in the core

of the tube wall; it thus works as if it had different heterogeneous layers due to two gradients: from inner surface to outer surface we have decreasing carbon and sulfur contents and the same happens for the quadrant facing the furnace center to the quadrant facing the furnace wall.

Table 3 - Chemical composition of used tube 1 cut and flattened, and chips machined

Sample Used 1 Thickness removed	Element (wt%)								
	C	Si	Mn	Cr	P	S	Ni	Mo	V
-	0,13	0,56	1,01	26,26	0,027	0,006	0,31	0,09	0,07
0,050mm	0,75	0,55	0,86	26,84	0,025	0,040	0,44	0,11	0,07
0,085mm	0,61	0,51	0,85	26,22	0,036	0,008	0,43	0.09	0,07
0,120mm	0,55	0,52	0,90	26,55	0,035	0,005	0,43	0,10	0,07
0,155mm	0,50	0,53	0,88	26,33	0,035	0,007	0,41	0,09	0,07
0,190mm	0,47	0,54	0,91	26,33	0,035	0,005	0,41	0,09	0,07
0,225mm	0,39	0,55	0,92	26,18	0,033	0,004	0,41	0,09	0,07
0,260mm	0,26	0,53	0,91	26,28	0,030	0,004	0,41	0,09	0,07
0,300mm	0,14	0,53	0,91	26,30	0,030	0,004	0,41	0,09	0,07
External side	0,13	0,53	0,92	26,27	0,031	0,005	0,41	0,09	0,07
Chips 0 to 1.5mm	0,179	-	-	-	-	0,092	-	-	-
Chips 1.5 to 3.0mm	0,141	-	-	-	-	0,012	-	-	-

Table 4 - Chemical composition of Used Tube 1 in each quadrant

Sample Used 1	Element (wt%)							
	C	Si	Mn	Cr	P	S	V	Mo
Quadrant 1 – facing center of furnace - I	0,78	0,53	0,70	25,48	0,056	0,033	0,09	0,15
Quadrant 2 – T	0,16	0,63	1,00	27,70	0,036	0,003	0,09	0,11
Quadrant 3 – facing furnace wall – O	0,13	0,63	1,00	27,50	0,037	0,003	0,09	0,11
Quadrant 4 – T	0,15	0,68	0,88	26,67	0,055	0,023	0,09	0,12

3.2- Microstructure before Heat Treatment

The microstructure of a new tube is composed of a ferritic matrix, with small carbides (Fig 3a). After use, the volume fraction and size of the precipitates have increased significantly. On the "bright-hotter" face (toward the chamber) the precipitates are blocky (Fig 3b), whereas on the hidden face (facing the wall) the precipitates look as contiguous colonies (Fig 3c). The SEM micrographs of the same samples are shown in Fig 4. The new tube 2 showed a particle of sigma phase, see arrow in Fig 4a, and EDS analysis revealed a Cr content of 51.8% consistent with the composition which confirms the sigma range. The used tube 1 (Fig 4b) presents the large particles which the EDS found to be carbides and the used tube 2 (Fig 4c) illustrates a micrograph of the hidden face where the amount of sigma is much higher according to EDS analysis. The EDS results are summarized in Table 5.

In Fig 5a, X-ray diffractogram from section of *new* tube is given. From this diffractogram, it is apparent that the microstructure of sample *new* consists of ferrite and Cr_2C. The sample *used* produces a similar pattern. This X-ray result was obtained by exploring the tube section which is small (tube thickness is 4.2mm when new and 4.0mm after use). To confirm the results, a piece of tube was flattened and the analysis was made on a much larger area of the tube internal surface after 0.3mm was removed by grinding. The X-ray result in Fig 5b show clearly the presence of sigma phase which forms on the hidden face of the used tube; on the "bright-hotter" face of the same tube no sigma was detected.

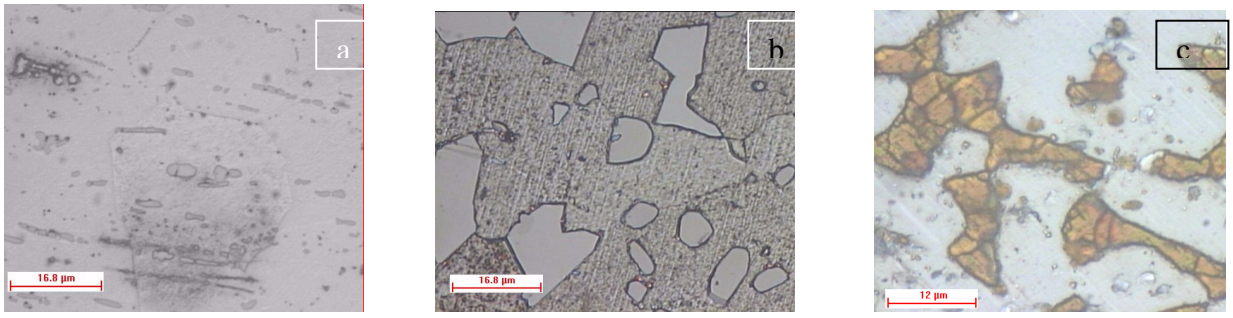

Figure 3 – Optical micrographs of: a) new tube 2, x800 glyceregia; b) used tube 1, bright face, x800 glyceregia and c) used tube 2, hidden face, x1000, electrolytic KOH.

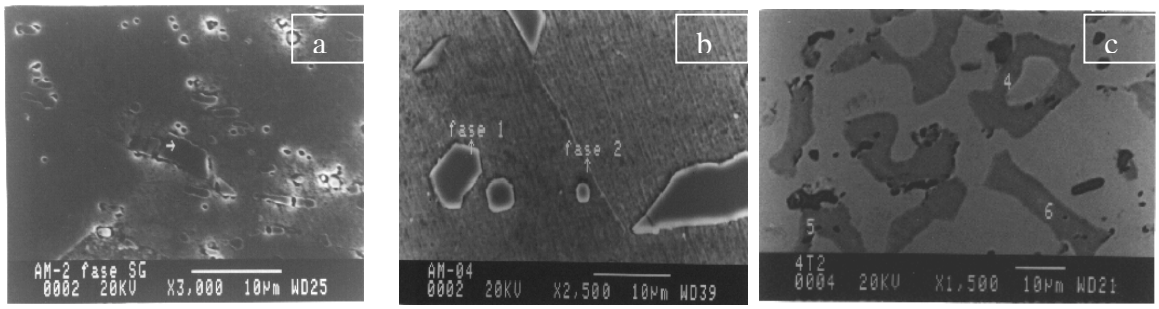

Figure 4 – SEM micrographs of: a) new tube 2, central region, glyceregia, x3000, b) used tube 1, surface region, bright face, glyceregia, x2500 and c) used tube 2, surface region, hidden face, electrolytic KOH, x1500.

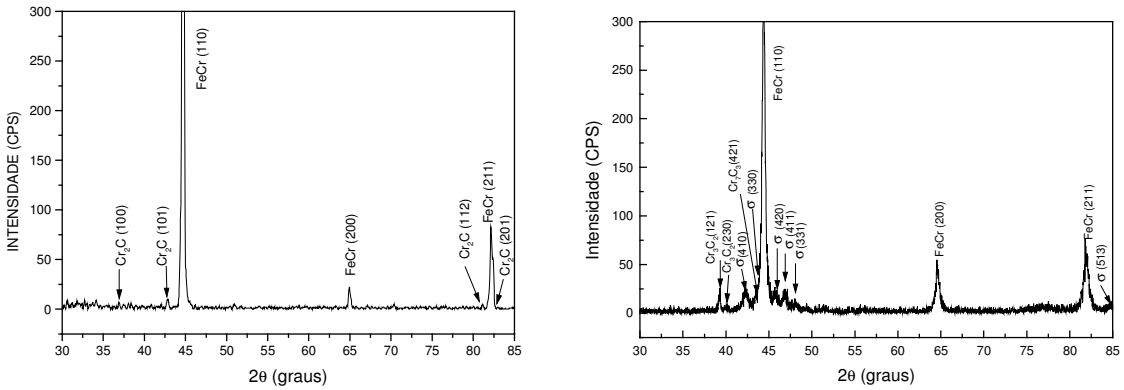

Fig 5- 5a- X-ray diffractogram (left) of sample *New 2* with 3 peaks of FeCr and ferrite and peaks for Cr_2C close to the main peak for ferrite. On the right side, a diffractogram for sample Used 1 after grinding 0.3mm. Several sigma peaks are apparent close to the main ferrite peak.

Table 5 - EDS results for new and used tube samples

Sample – Particle	Element (wt%)				Identification
	Cr	Si	Mn	V	
New2- long dark particle	51.83	0.25	0.50	0.59	Sigma
New2- round particles	73.08	0.19	0.76	1.48	CrV carbide
Used1- large particle	80,71	0.0	0.82	0.00	Cr carbide
Used1- small particle	91.97	0.0	1.26	2.67	CrV carbide
Used2 – large gray particles (6)	35.23	1.40	2.03	0.12	Sigma
Used2 – dark particles	84.62	0.22	1.01	0.05	Cr carbide

3.3- Microstructure after Heat Treatment

After heat treatment, the used tube samples exhibited similar structures for both, water and air cooling. The samples from the bright face contained only carbides at the surface and a small amount of sigma phase in the central region of the tube wall. Fig 6 shows a sample which was heated to 900°C and kept there for one hour. The sigma phase is dissolving while the carbides remain unchanged. Increasing the time at 900°C up to 108h does not alter the carbide distribution. The effect of increasing temperature for samples taken from the bright face for a homogenization time of 2h was determined by a series of treatments starting with 850°C and going up to 1300°C.

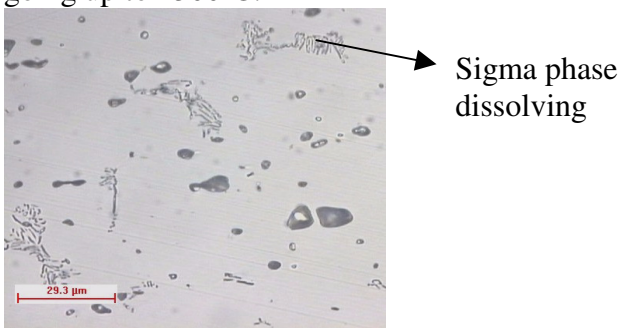

Figure 6 -Optical micrograph of Used Tube 1, central region, bright face, x400, electrolytic NaCN.

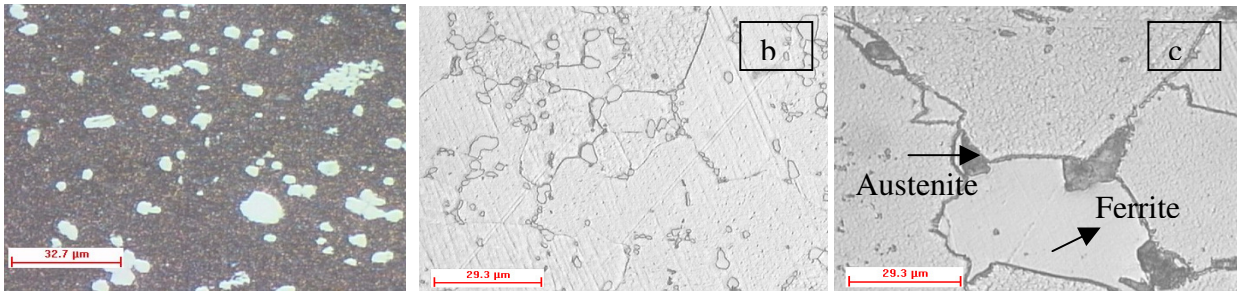

Figure 7. Optical micrographs of used tube 1, heat treated for 2 hours at different temperatures, all samples from bright face and x400: a) 850°C, central region, Fry's reagent; b) 1000°C, central region, glyceregia and c) 1300°C, central region, glyceregia.

At 850°C and in the surface region, no sigma phase was observed, whereas, in the center (Fig. 7a) the sigma phase appears to be dissolving. At 1000°C no sign of the sigma phase remains (Fig 7b) although the carbides are still present. The grain and carbide size increase with temperature until 1150°C. At 1300°C (Fig 7c), all the carbides dissolved. The different color for the grains is due to the diffusion of carbon into the inner parts of the sample and the simultaneous appearance of austenite; this has also been reported by Demo(1) who proposed the following sequence: regions high in carbon transform to austenite when annealing. Upon cooling to form martensite, further annealing at 650°C tempers the martensite and causes chromium carbide to precipitate. Fig 7 shows a sequence of three temperatures for the treatment.

Another sequence was experimented with using samples from the hidden face with temperatures varying from 850°C to 1200°C. Fig 8 below shows the micrographs. At 850°C, the presence of sigma phase is noted both at the surface and the center, but only at the surface is some dissolution observed. As the temperature is raised the sigma dissolves and at 950°C it is completed. Above 950°C, the carbides tend to concentrate at grain boundaries and their total volume decreases. At 1100°C, the presence of austenite is noted, increasing time to 60h causes

grain coarsening, but the carbides are still stable, which is in accordance to the work of Aksoy(6) for 18%Cr ferritic stainless steels, and at 1200°C the carbides are dissolved.

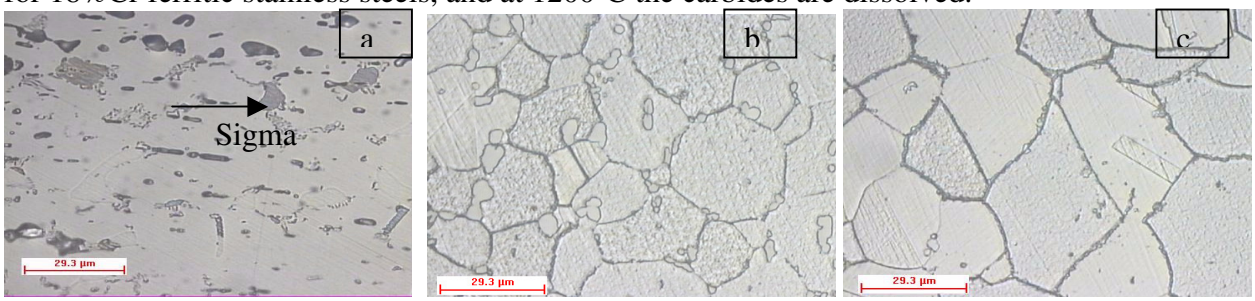

Fig 8 – Optical micrographs of used tube 2, heated at different temperatures, all samples from hidden face: a) 850°C, 1h, surface region, electrolytic NaCN, x400; b) 1100°C, 2h, surface region, glyceregia, x400, c) 1200°C, 2h, surface region, glyceregia, x400.

The EDS analysis, shown in table 6 confirms the presence of sigma phase at temperatures of 850, 900 and 930°C while, above 950°C, the phase is dissolved. This temperature range is slightly higher than those reported elsewhere (2,7,8) and it might be due to the working conditions that resulted in carburization and sulfidation, and the consequent modification in the chemical composition and dissolution characteristics. The study confirmed that increasing carbon diminishes the tendency for sigma formation, by tying up the carbon as carbide (2).

Table 6 - EDS results for heat treated samples, illustrated in Figure 9

Tube	Sample – Particle	Element (wt%)				Identification
		Cr	Si	Mn	V	
U2	HT at 850°C–large center phase	38,02	0,99	1,86	0,00	Sigma
	-Dark round phases	78,26	0,06	1,45	0,12	Cr carbide
	HT at 900°C –bright phase	29,12	0,10	2,71	0,19	Cr carbide
	-small black phase	59,26	0,06	4,02	0,15	Sigma in dissolution
U3	HT at 930°C – large phase in center	44,81	0,57	1,42	0,58	Sigma in dissolution
	-Dark phase to the right	87,64	0,28	0,86	2,38	CrV carbide
	HT at 1000°C – “C3” phase	64,98	0,32	1,21	1,07	CrV carbide
	HT at 1100°C – “E” phase	88,76	0,20	0,61	2,19	CrV carbide

The SEM images for the heat treated samples are shown in Fig 9. In Fig 9a the precipitate is identified as sigma (the chromium content of 38,0% confirmed that). In fig 9b we see a region similar to the one in fig 9a (arrow A), however the chemical composition is the same as in the matrix, the dark spots have a chromium of 29% indicating that in this region solubilization of sigma is occuring. Figs 9c and d show the same sample region with different magnification, the arrow shows a sigma particle in the final stages of solubilization. In Fig 9e arrow **b** shows a carbide with 79% chromium and e 1,7% vanadium. The carbide identified by **C3**, have presented 65% chromium and 1,0% vanadium, and the carbide identified by arrow **d** had 75% chromium and 0,2% vanadium. In Fig 9f carbide **b** has 70% chromium. In the column “identification” of tables 5 and 6 we defined CrV as the carbides which showed a rounded morphology, chromium above 79% and vanadium above 1,4%.

In Figure 10 X-ray diffraction of tubes after heat treatment, indicates the presence of $M_{23}C_6$ carbides (Fig 10a), and no sigma indication. The samples treated at higher temperatures show the presence of austenite as seen in Fig 10b. At 1200°C the carbides are dissolved, although the x-

ray diffraction shows the presence of some $Cr_{23}C_6$ and C_7C_3, which is attributed to precipitation on cooling.

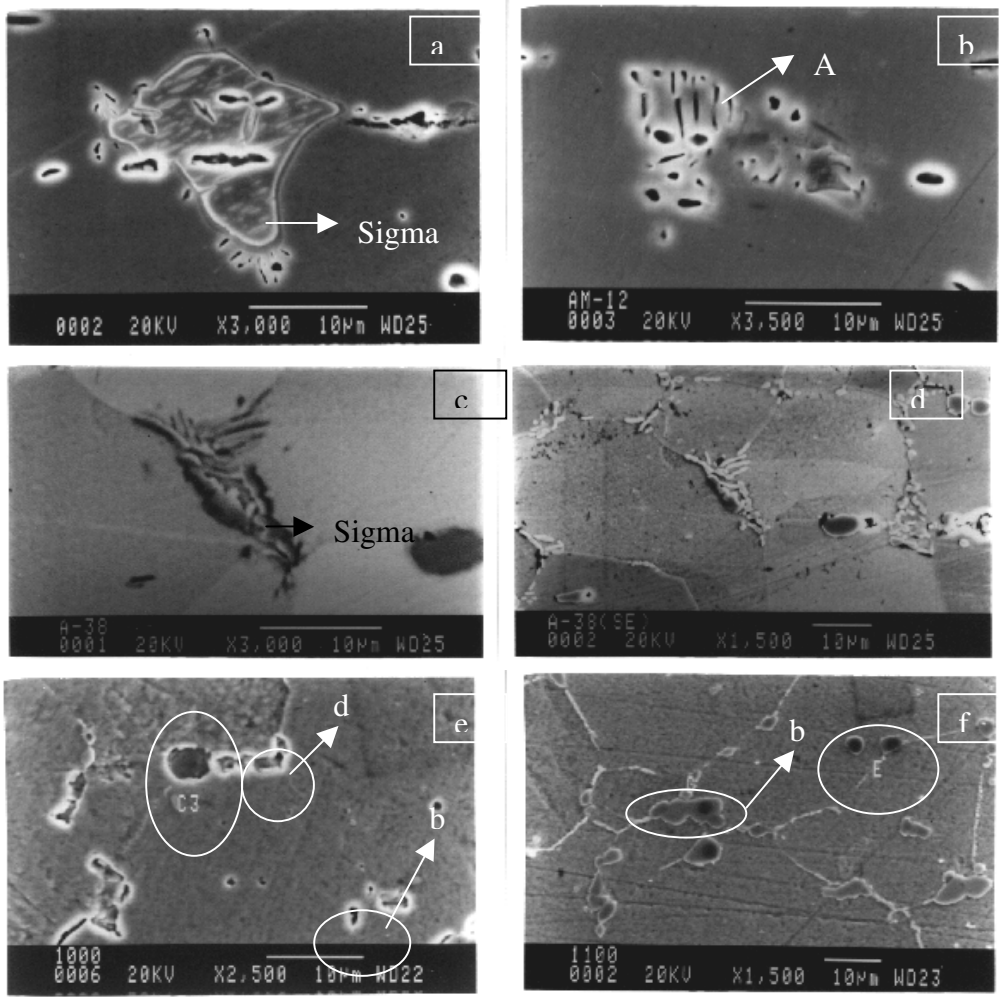

Fig 9 - SEM micrographs of used tubes, hidden face, after heat treatment: a) 850C, 1h, central region, electrolytic KOH, x3000, b)900C, 2h, central region, electrolytic KOH, x3500, c) 930C, 2h, central region, glyceregia, x3000, d) 930C, central region, glyceregia, x1500, e) 1000C, 2h, central region, electrolytic KOH, x2500 and f) 1100C, 2h, central region, glyceregia, x1500.

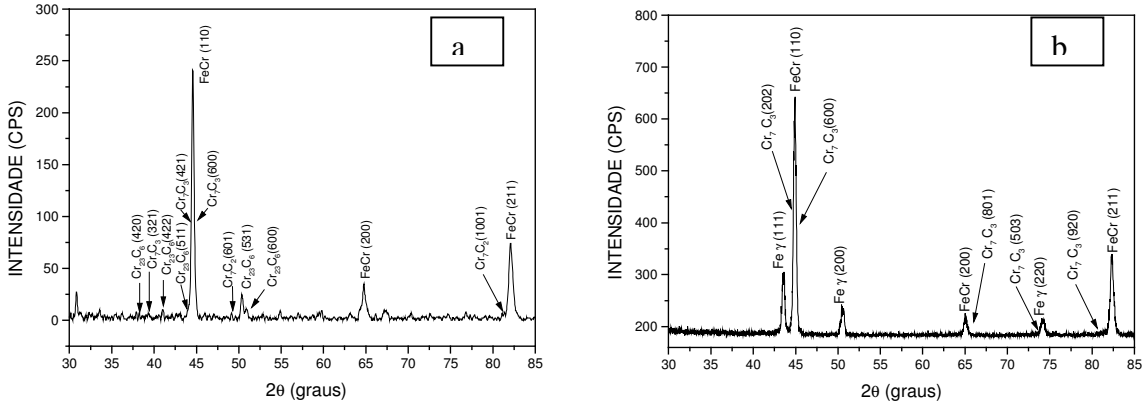

Fig 10 – X-ray diffractogram of a sample of used tube 1, treated at 850°C for 1h (left), and at 1200°C for 2h (right). Austenite peaks appear at 1200°C. No peaks for Sigma were found.

From the chemical composition, it is possible to calculate the maximum amount of carbides that could precipitate. It has also been possible to predict the precipitation of carbides and sigma through computerized calculations (9) in austenitic alloys. According to Linus Pauling's (10) electron hole theory, it is possible to calculate the electron hole number Nv of an alloy. For the steel studied the following Nvs were found – Table 7.

Table 7 – Calculated values for Nv

Sample	Carbon (wt%)	Nv	Likeness of sigma formation
New 2	0,089	2,822	Yes
Used 2	0,13	2,810	Yes
Used 2 – Quadrant 1	0,78	**2,234**	**No**
Used 2 – Quadrant 2	0,16	2,863	Yes
Used 2 – Quadrant 3	0,13	2,887	Yes
Used 2 – Quadrant 4	0,15	2,850	Yes

If the values are above 2,45-2,50 the alloy is prone to form sigma, if Nv is below 2,45-2,50 the alloy is considered safe(11). The results are confirming our observations since sigma was not found in the samples with high carbon content.

3.4- Hardness and microhardness

Table 8 – Results of microhardness

Tube	**Sample**	**Region and Position**	**Measure site**	**Figure**	**Identifi-cation**	**Micro HV**	**RB equiv.**
U1	Used 1	O - SI	Matrix	4a	Ferrite	250 ± 15	99,5
	Used 1	O - SI	Precipitates	4a	Sigma	944 ± 37	*ND
U2	Used 2	I – SI	Matrix	4b	Ferrite	222 ± 13	95,5
	Used 2	I – SI	Phase 1	4b	Carbide	917 ± 31	ND
	Used 2	I - SI	Phase 2	4b	Carbide	1816 ± 200	ND
U3	Used 3	O – CE	Matrix	3c	Ferrite	254 ± 12	100
		O – CE	Orange Phase	3c	Sigma	673 ± 27	ND
		O – CE	Whitish phase	3c	Carbide	1226 ± 78	ND
U3	Used 3	O – SI	Matrix	4c	Ferrite	201 ± 7	91.7
		O – SI	Phase "6"	4c	Sigma	954 ± 23	ND
		O - SI	Phase "4"	4c	Carbide	1031 ± 26	ND
U2	Treated at 850°C	O – CE	"Phantom" Phase	9a	Sigma	973 ± 175	ND
		O – CE	Dark phase	9a	Carbide	1432 ± 131	ND
		O – CE	Bluish phase	8a	Sigma	522 ± 43	ND
		O – CE	Matrix	9a	Ferrite	215 ± 11	94,2
U1	Treated at 900°C	I – CE	Lamelar region	6	Ferrite	180 ± 4	87,1
		I - CE	Matrix	6	Ferrite	213 ± 4	93,8
U2	Treated at 900°C	O - CE	Lamelar region	9b	Ferrite	228 ± 14	96,4
		O - CE	Matrix	9b	Ferrite	214 ± 10	94,1
U3	1000	I - CE	Matrix	9e	Ferrite	198 ± 9	91.3
	1100	O - CE	Matrix	9f	Ferrite	210 ± 11	93.4
	Treated at 1300°C	I – CE	Dark grains	7f	Austenite	321 ± 15	ND
		I - CE	Light grains	7f	Ferrite	207 ± 10	93.0

SI – internal surface, CE – central region *ND = no equivalent hardness on this scale.

Hardness measurements were taken for several samples: for new tubes we found values averaging 87HRB; for used tubes the average was 85HRB; for samples treated and air cooled the average was 87HRB and for samples treated and water cooled the average was 92HRB. The significant data is that water cooled samples presented higher hardness values than those air cooled. The samples from new or used tubes had basically similar values (84 to 88 HRB).
Micro hardness results are given in table 8.

The sigma phase hardness results found are in agreement with that reported by Wolff (12), who measured 940HV. The lower value we found, of 522HV is explained by the chromium content of 38% which indicates that we are in the sigma- alfa field of the chromium-iron diagram, with the resultant lower hardness.

The ferritic matrix is reported in the literature with hardness going from 111 to 339HV (1,8,12 and 13). The values we had are within this range (from 176 to 254HV).

The carbides had hardness varying from 917 to 1816HV. Brandis (14) has related for $M_{23}C_6$ a hardness of 1250HV. This indicates that we might have different carbides, which was confirmed by the X-rays diffraction.

4- CONCLUSIONS

(1) Two phases precipitate during use: chromium carbides in the surface region of the bright face (region facing the burner flame –temperature around 750^{o}C) and the sigma phase on the hidden face (region opposite to the flames –temperature around 650^{o}C). In the central region of tube wall, no matter which face we look, there is sigma and carbide precipitation.

(2) The effect of the carbon content is significant: precipitation of carbides is preferential when the carbon is above 0,20% and Nv values are below 2,5. Under this condition, the carbide effect is the important factor for the tube performance. If carbon is below 0,20% sigma phase can occur.

(3) Sigma phase dissolution is possible and under the conditions studied is complete at 900^{o}C after 4 hours or 950^{o}C after 2 hours. The carbides were all dissolved after 2 hours at 1200^{o}C.

(4) The microstructure of tubes varies considerably from one position to another. Due to the furnace and process design, the gases passing inside the tube promote the carburization and sulfidation in the internal surface of the tubes. Since there is a temperature gradient from the bright and hidden face of tubes which can go as high as 120^{o}C, the absorption of these elements is much higher at the bright face than at the hidden face. The higher the carbon absorption the higher the carbide formation and chromium depletion of the matrix with deleterious influence to corrosion and mechanical properties. The tubes fail preferentially at the bright face due to the chromium depletion, which favors the sulfidation even more.

ACKNOWLEDGEMENTS

The authors would like to thank Petrobras for the financial support, Villares Metals for the chemical analysis made and Prof. Michael Kaufmann from University of Florida for the proof reading of this paper.

REFERENCES

1- Demo, J.J. - Structure, constitution, and general characteristics of. Wrought ferritic stainless steels - ASTM STP 619, 1977, 1-65.

2- Smith, G.V. – Sigma phase in Stainless – Iron Age, November, 1950, p 63-68.

3- Souza F.,B.G.; Paiva, G.J.M. e Goulart, R.A. ; Avaliação das falhas dos tubos do Forno F-23001 da SIX – CT SEMEC 21/98, Fevereiro de 98, 22p.

4- Souza F., B.G. e Goulart, R.A. ; Comportamento em fluência de aço inox ferrítico usado nos tubos do forno F-23001 da SIX – CT SEMEC 117/98, Setembro de 1998, 25p.
5- Nogueira Jr, L.; e Souza, E.J.J.; Análise da serpentina de radiação do forno F-23001 da SIX – Janeiro de 1994, 44p.
6- Aksoy, M., Kuzucu, V. and Korkut, M.H. - The influence of strong carbide-forming elements and homogenization on the wear resistance of. Ferritic stainless steel, Wear, 211, (1997), 265-270.
7- Brown, E.L. et alii - Intermetallic phase formation in 25Cr-3Mo-4Ni ferritic stainless steel, Met.Trans. A, vol 14^{A}, May 1983, pp791-800.
8- Van Zwieten, A.C.T.M. and Bulloch,J.H.; The influence of Interstitial Solute Level on The Charpy Toughness Properties of a 40% Cr-Fe Stainless Steel, Int.J.Ves.& Piping, 56, (1993), 69-91.
9- Sims, C.T. - Prediction of Phase composition, Superalloys II, John Wiley & Sons, Inc. 1987, pg217.
10- Pauling, L.; Phys. Rev., 54, 899 (1938).
11- L. R. Woodyatt, C. T. Sims and H. J. Beattie, Jr., (1966), TMS-AIME, v. 236, p.519.
12- Wolff, I. M., (1992), Premachandra, K. And Cortie, M.B. –Second Phase Particles in Ferritic Steels Containing 40% Chromium, Mat. Characterization, 28, p. 139-148.
13- Nichol, T.J., Datta, A. and Aggen, G., (1980), Embrittlement of Ferritic Stainless Steels, Met. Trans A, v. 11A, p. 573-585
14- Brandis, H. et al., T.E.Tech.Ver., Special Issue, 5, (1983).